A scintillator plus silicon photomultiplier heavy-ion detector array for g-factor measurements by the time-differential recoil-in-vacuum method

Jack Woodside[1,*], *Andrew* Stuchbery[1,**], *Brendan* McCormick[1], *Georgi* Georgiev[2], *Tom* Kitchen[1], *Daniel* Tempra[1], *Jack* Pidgeon[1], *Safiya* Badri[1], *Josh* Herridge[1], *Ben* Coombes[1], *Gregory* Lane[1], and *AJ* Mitchell[1]

[1]Department of Nuclear Physics and Accelerator Applications, Research School of Physics, The Australian National University, Canberra, ACT 2601, Australia
[2]IJCLab, CNRS/IN2P3, Université Paris-Saclay, 91405 Orsay, France

Abstract. A plunger device is being developed at the Australian Heavy Ion Accelerator Facility to perform g-factor measurements using the time-differential recoil-in-vacuum technique. The target chamber housing the device includes an array of particle detectors with an integrated amplification circuit. The array consists of 24 cerium-doped lutetium-yttrium oxyorthosilicate (LYSO:Ce) crystals coupled to silicon photomultipliers, configured into two rings. The array was tested with a light source, an α-particle source, and a heavy ion beam in order to examine the performance and stability of the device under vacuum. Thermal equilibrium was reached quickly, and the array showed no signs of signal degradation after an extended period of use. The rate dependence and mass dependence of the output was tested in beam.

1 Introduction

Large-basis shell-model calculations generally describe the low-excitation structures of fp-shell nuclei well. One experimental observable that can be examined is the g factor, which gives a sensitive test of the proton versus neutron character of the nuclear states. There are extensive data on the first-excited states of even-even nuclei in the fp shell measured by the transient-field technique [1], however the current recommended values of most of these g factors have uncertainties increased above those reported by about ±15% to account for uncertainty in the transient-field strength. The difficulty in calibrating the transient-field strength is due to a lack of suitably precise independently known g factors for nuclei with atomic numbers $14 < Z < 40$ [2].

One possible way to provide applicable calibration g-factor values is to use the time-differential recoil-in-vacuum (TDRIV) method [3, 4] for ions with a Na-like electron configuration [5, 6], for which the hyperfine interactions can be calculated precisely [6, 7]. This approach requires use of a plunger device [8]. The device consists of two parallel foils, with a mechanism to adjust the distance between them precisely. Once the nuclei of interest have been created via a suitable nuclear reaction in the first 'target' foil, they recoil through the vacuum towards the second 'stopper' foil. The hyperfine fields from the recoiling ion's electron configuration will couple with the nuclear spin, causing the nucleus to precess about the coupled spin with a frequency proportional to the g factor of the state, until the ion is stopped in the second foil. This precession can be observed via the attenuation in the angular correlation of the emitted γ rays. Varying the distance between the foils allows the observation of the time dependence of the nuclear precession, which in turn allows the measurement of the g factor, based on calculated atomic hyperfine-field strengths [7].

An experimental setup for performing TDRIV measurements is currently being developed at the Australian Heavy Ion Accelerator Facility. The objective is to perform precise reference measurements for a range of nuclei, thus providing crucial calibration values for a large set of both past and future g-factor measurements. Initial experiments will use particle-γ angular correlations following the Coulomb excitation of the nuclei of interest. Thus, the plunger must be provided with a particle-detector array, which both provides particle-γ coincidence information, as well as determining the kinematics of the reaction.

This paper focuses on the design and testing of the particle-detector array. First, the thermal characteristics of the design were tested using an external light source to activate the silicon photomultipliers (SiPMs). Second, an α source was used to test the performance of the scintillators coupled to the SiPM and amplifier circuit. Finally, an in-beam test was performed to characterise the array's performance with a range of beam conditions.

2 Detector Design

A model of the front and back of the PCB that contains the SiPMs and amplification circuitry can be seen in Fig. 1, with the main features labelled.

The particle detector array consists of a 24-unit circular array of 6 mm × 6 mm SiPMs. These units are arranged

*e-mail: jack.woodside@anu.edu.au
**e-mail: andrew.stuchbery@anu.edu.au

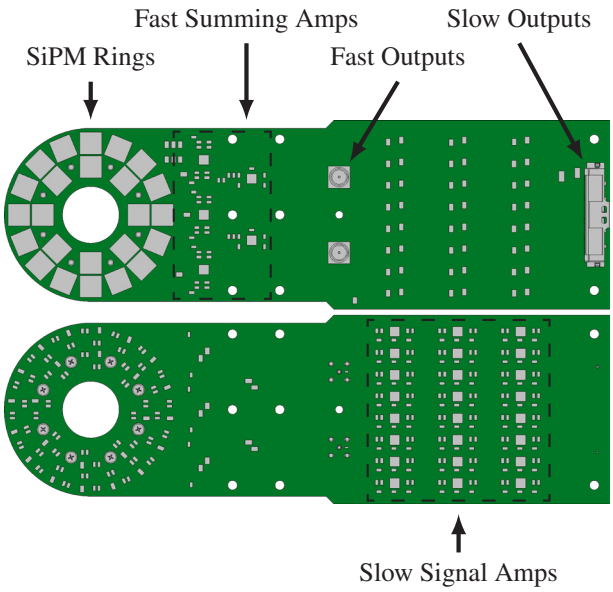

Figure 1. Design of the PCB used for the particle detector array highlighting the key components.

into two rings, with the inner ring containing 8 SiPMs, and the outer ring containing the remaining 16 SiPMs. The SiPMs used in the array are MICROFC-60035-SMT C-series SiPMs from onsemi [9]. The microcells in the SiPMs are 35 μm, with 18,980 microcells per SiPM, and the recovery time for the microcells is 95 ns. This model was chosen as the C-series SiPMs uniquely have a separate 'fast' output for timing.

These SiPMs each have a 'slow' and a 'fast' output, which can be used for energy and timing resolution, respectively. Each slow output is amplified individually by an Analog Devices AD8066 op-amp [10]. The fast outputs are connected together in sets of 4 using signal-driven multiplexing (SDM) by pairs of Schottky diodes (see, for example, Ref. [11]). Using SDM as opposed to directly summing the outputs reduces coupling between the detectors as only active SiPMs are connected to the common output at a time, reducing signal degradation. The SiPMs were multiplexed in groups of 4 by Infineon BAT15-04W diode pairs [12], which were then summed and amplified using Analog Devices AD8012 op-amps [13].

Each of the 24 SiPMs is coupled to a single 6 mm × 6 mm × 0.5 mm scintillator. The scintillator chosen was LYSO:Ce due to its high light output and fast decay time, while also having moderate energy resolution. In particular, the fast decay time allows for both good timing resolution and high rates. The emission peak of LYSO is 420 nm, which matches the peak wavelength of the SiPMs. The scintillator crystals were not wrapped with a reflector, and were coupled to the SiPMs using UV-cured optical adhesive. The specific adhesive used was Norland Optical Adhesive 68 (NOA 68), which transmits 420 nm light well.

3 Tests

3.1 Thermal Testing

Since the gain of SiPMs is temperature dependent and both the SiPMs and the op-amps produce heat, the temperatures of various components while powered and under vacuum were measured using two K-type thermocouples. The thermocouples were attached either to the outside casing of the op-amps, or the edge of the SiPM housing. In these tests the scintillator was not used, and the SiPMs were activated directly by LED pulses.

The op-amps heated rapidly, reaching temperatures of over 70°C. This is not a problem for the op-amps, but since the circuit is under vacuum the heat conducts through the PCB towards the SiPMs which reached 40°C. This temperature increase causes the SiPM gain to drop, until the signal is no longer visible above the baseline noise level. As a remedy, a copper heat sink was added over the op-amps, together with heat pipes to conduct the heat away to the chamber wall. A significant temperature decrease was achieved, as can be seen in Fig. 2. The system reached an equilibrium of around 30°C in about 15 minutes. Testing with a LED indicated no further loss of SiPM signal once equilibrium was reached, and there was no evidence of temperature change when the LED was turned off and on.

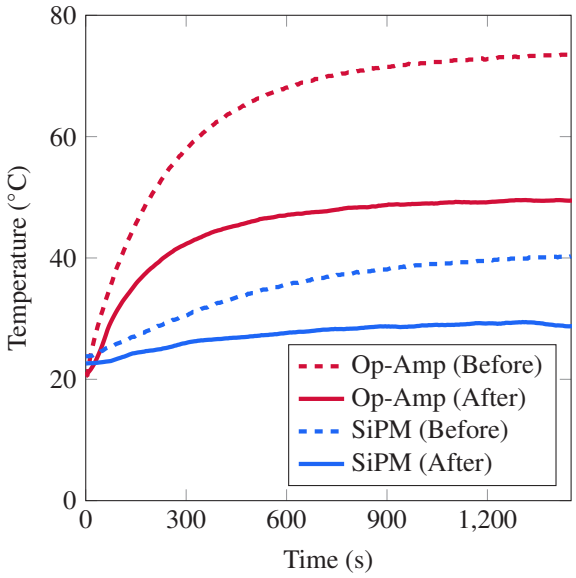

Figure 2. Heating of the PCB components whilst powered and under vacuum before and after the heat sink was added.

Self-heating of SiPMs has been investigated previously by Wang *et al.* [14] using GAGG scintillators and 3×3 mm^2 SiPMs from the same manufacturer. They used a ^{137}Cs source, and measured the energy spectrum at temperatures from 0°C to 40°C. Their results suggest that temperature fluctuations of 2°C around 30°C would result in less than a 5% variation in the SiPM gain. This variation is not significant in our application.

3.2 α-Source Testing

Once the thermal heating of the SiPMs was controlled, an α-particle source was used to test the scintillator performance, and examine the energy spectra produced by the SiPMs. An ^{241}Am source was placed approximately 5 cm away along the centre axis of the rings. Data were collected using an XIA Pixie-16 digital data acquisition system.

With the energy resolution of the LYSO, an ^{241}Am source should produce a single Gaussian peak at an energy of approximately 5.5 MeV [15]. However, a three-Gaussian structure was observed, as shown in Fig. 3. The relative

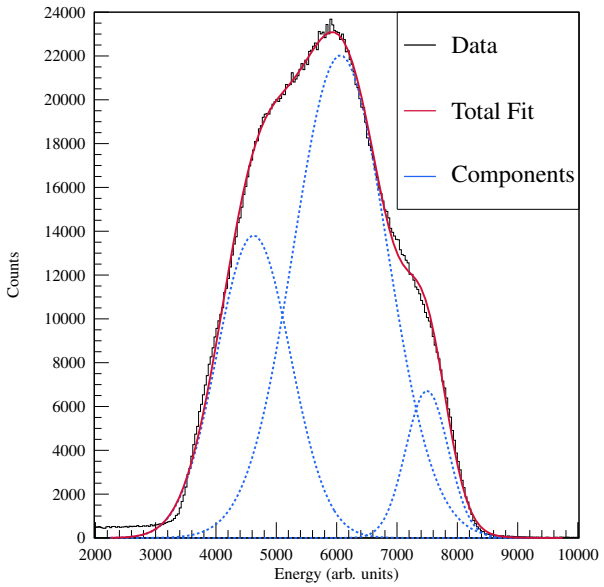

Figure 3. The ^{241}Am energy spectrum as measured by the LYSO/SiPM. A three-peak structure can be clearly seen due to optical effects based on where the particle impinges on the LYSO.

heights of the peaks varied from detector to detector, but the distinctive shape remained.

This effect has been seen previously by Luo *et al.* [16], who also used LYSO crystals of a similar size on SiPMs with an ^{241}Am source. They also see a three-Gaussian structure, although in their spectra the 'shoulders' either side of the central peak appear to be the same height. The height differences are likely due to the source position, which for their experiments was centred on the detector, whereas our source was centred on the ring. They attribute the structure to the location in the scintillator where the α particle interacts. When they placed a mask with a 1 mm collimator over different parts of the scintillator, they could see three distinct peaks at different energies for the centre, edge, and corner of the scintillator. This observation was also backed up by simulations.

To make similar measurements, masks were 3D printed to block parts of the scintillator surface. The masks were printed with polylactic acid, were 2-mm thick, and had 2 mm $\times$ 2 mm square collimators over either the centre or the corner of each detector. While these collimators are larger than those used by Luo *et al.*, and more than one region of the scintillator may be exposed, they should still change the relative heights of the three components.

The components were not as clearly separated as those seen in Ref. [16]. This is likely due to the different collimator sizes, as well as potentially light reflecting from the back of the masks. Despite this, there were still qualitative differences in the height variation across the peak structure, suggesting a position-dependent response.

The structure in the peak is likely to originate from optical effects, depending on where in the scintillator the α particle interacts. This effect might be resolved by wrapping the scintillators in a reflective coating so that all the photons are directed towards the SiPM rather than some escaping. However, since the detectors are only being used as a trigger for coincidence events rather than precise energy measurements, this peak structure is not expected to prevent the use of this detector array in the proposed TDRIV experiments.

One other effect, which could cause problems, is optical crosstalk caused by some light from one scintillator being detected by an adjacent SiPM. It is straight forward to check for crosstalk by looking for coincident events between (adjacent) detectors; no evidence of cross talk was found in our tests.

3.3 In-Beam Testing

The array was tested using heavy ion beams. The measurements were performed at the Heavy Ion Accelerator Facility at the Australian National University. Beams of ^{74}Ge at several energies up to 180 MeV impinged upon a 200-μg/cm^2-thick target of $^{\text{nat}}$C. The array was placed approximately 2 cm downstream of the target and centred on the beam axis.

A High-Purity Germanium (HPGe) detector was placed at 45° to the beam. Signals from the HPGe detector and the particle detectors were processed by an XIA Pixie-16 digital data acquisition system. The data were acquired in list mode with no coincidence trigger condition, then processed to construct coincidence events using a coincidence window of 3 μs.

Forward-scattered carbon ions with energies up to $\approx$ 60 MeV were detected in the scintillator array. Their energies varied as expected as the beam energy was varied, however a significant dependence of the gain on count rate was observed. Measurements were taken with approximately 0.5 kHz, 1.5 kHz, and 3 kHz per SiPM, and are presented in Fig. 4.

As the rate increases, the peak position moves to a lower energy. The peak appears to narrow at higher rates, but the width relative to the centroid position remains constant, so the resolution does not actually vary. Since the particles still have the same real energy, this is possibly due to the microcells in the SiPM not having recovered at higher rates, leading to fewer photons being detected and a 'lower' energy being measured. It could also be caused by the amplification circuit, which might give rise to effects such as a longer recovery time or higher baseline at higher rates. These possibilities will be investigated in future work by examining the waveforms as the rate varies. As the rates

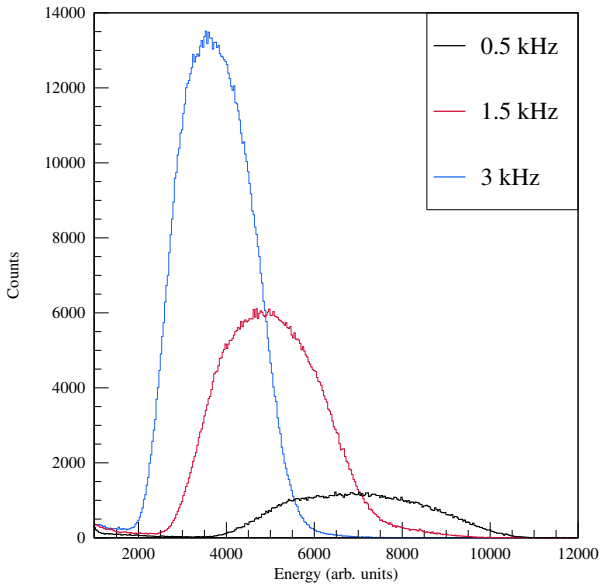

Figure 4. The energy spectrum of the ^{74}Ge beam as measured by the LYSO/SiPM at different particle rates per SiPM. There is a clear dependence on the rate for the peak centroid.

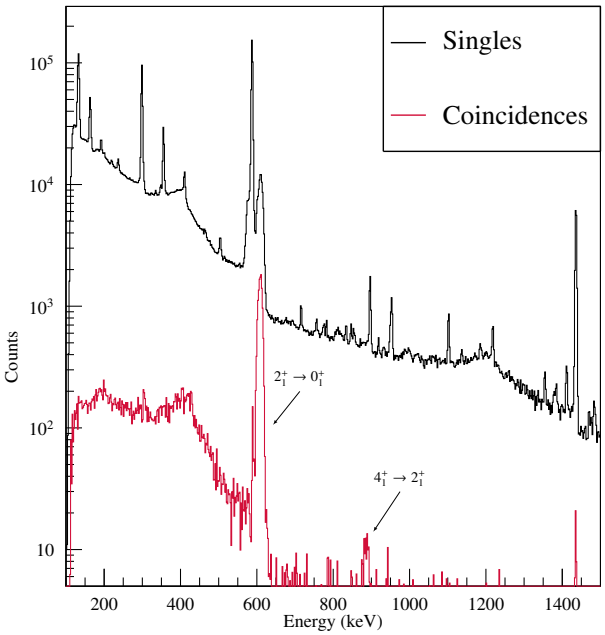

Figure 5. Singles and coincidence γ-ray spectra from the HPGe detector during the heavy ion beam measurement. Contaminant γ rays in singles are primarily from room background and Coulomb excitation of the tantalum collimator and beam stop.

are not expected to vary significantly during an experiment, and are generally lower in the proposed experiments than those used in these tests, the rate-dependent behaviour is not of great concern.

The particle-γ time differences showed a clear prompt peak, which was gated on with a random background subtraction set from both sides of the prompt peak. The γ-ray singles and particle-γ coincidence spectra for the 180-MeV ^{74}Ge beam are shown in Fig. 5. Two transitions from ^{74}Ge [17] were identified. The other peaks in the spectrum are from either ^{181}Ta Coulomb excitation of the collimator and beam stop [18], or room background. In the coincidence spectrum, the peak-to-background ratio of the 596-keV peak from the $2_1^+ \rightarrow 0_1^+$ transition in ^{74}Ge has improved significantly, and the contaminant γ rays have been essentially removed. In particular, the strong stopped peak from ^{74}Ge Coulomb excitation on the collimator and beam stop has been eliminated. The smaller 868-keV peak from the $4_1^+ \rightarrow 2_1^+$ transition is more apparent after the gating. There is still a Compton background present and a small residue of the ^{40}K peak from room background, however the plunger device and particle detector will eventually be used with a shielded and Compton-suppressed HPGe array, which will reduce both. The beam stop can also be moved further downstream out of view of the γ-ray detectors, reducing the ^{181}Ta Coulomb excitation peaks.

The $2_1^+ \rightarrow 0_1^+$ yields can then be extracted from the particle-gated γ-ray spectrum for each particle-γ combination and corrected for the particle detection efficiency (there was a single HPGe detector in this test run). From these data we can fit a standard angular correlation function $W(\theta)$, where $W(\theta) = 1 + a_2 P_2(\cos\theta) + a_4 P_4(\cos\theta)$, and θ is the angle between the carbon recoil and the γ-ray, assuming detection at the average detection angles. An example is shown in Fig. 6 for the inner ring. This function is an

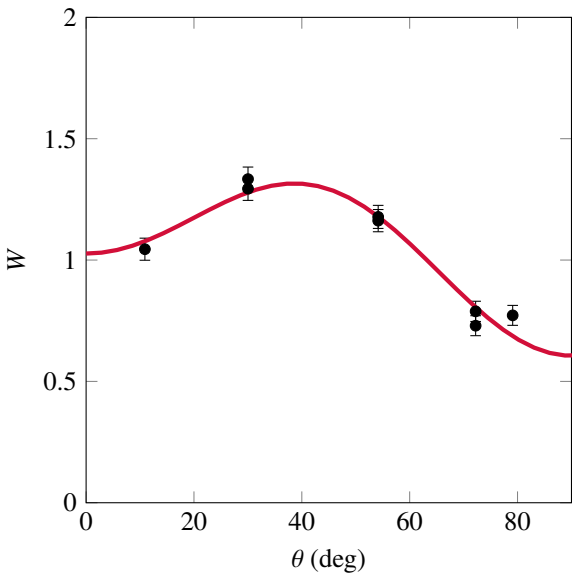

Figure 6. Angular correlation of the $2_1^+ \rightarrow 0_1^+$ transition for the inner ring of particle detectors. Note that points with the same angle difference agree with each other.

approximation which does not take into account relativistic effects, but the general shape of the correlation is as expected and the data are clearly self-consistent.

4 Conclusions

A new particle-detector array has been developed for use in time-differential recoil-in-vacuum measurements. The device has been tested both with an α-particle source and

with heavy ion beams. The heat sink for the amplification circuit allows stable operation under vacuum for extended time periods, and the particle detectors have been shown to provide the coincidence and kinematic information required for the TDRIV method.

Acknowledgements

J. A. Woodside acknowledges support of the Australian Government Research Training Program Scholarship. This material is based upon work supported by the Australian Research Council Grant Nos. DP17010673, DP210101201, and DP250100400. The authors acknowledge the facilities, and the scientific and technical assistance provided by Heavy Ion Accelerators (HIA). HIA is supported by the Australian Government through the National Collaborative Research Infrastructure Strategy (NCRIS) program.

References

[1] N.J. Stone, Table of Recommended Nuclear Magnetic Dipole Moments: Part II, Short-lived States, IAEA Nuclear Data Section (2020). 10.61092/iaea.1p48-p6c6

[2] M.C. East, A.E. Stuchbery, S.K. Chamoli, A.N. Wilson, H.L. Crawford, J.S. Pinter, T. Kibédi, P.F. Mantica, g factor of the first excited state in ^{56}Fe and implications for transient-field calibration in the Fe region, Phys. Rev. C **79**, 024303 (2009). 10.1103/physrevc.79.024303

[3] A.E. Stuchbery, P.F. Mantica, A.N. Wilson, Electron-configuration-reset time-differential recoil-in-vacuum technique for excited-state g-factor measurements on fast exotic beams, Phys. Rev. C **71**, 047302 (2005). 10.1103/physrevc.71.047302

[4] A. Kusoglu, A.E. Stuchbery, G. Georgiev, B.A. Brown, A. Goasduff, L. Atanasova, D.L. Balabanski, M. Bostan, M. Danchev, P. Detistov et al., Magnetism of an Excited Self-Conjugate Nucleus: Precise Measurement of the g Factor of the 2_1^+ State in ^{24}Mg, Phys. Rev. Lett. **114**, 062501 (2015). 10.1103/physrevlett.114.062501

[5] A.E. Stuchbery, B.P. McCormick, T.J. Gray, B.J. Coombes, Pushing the limits of excited-state g-factor measurements, EPJ Web Conf. **178**, 02005 (2018). 10.1051/epjconf/201817802005

[6] B.P. McCormick, A.E. Stuchbery, A. Goasduff, A. Kusoglu, G. Georgiev, Modelling hyperfine interactions for nuclear g-factor measurements, EPJ Web Conf. **232**, 04009 (2020). 10.1051/epjconf/202023204009

[7] C. Froese Fischer, G. Gaigalas, P. Jönsson, J. Bieroń, GRASP2018—A Fortran 95 version of the General Relativistic Atomic Structure Package, Comput. Phys. Commun. **237**, 184 (2019). 10.1016/j.cpc.2018.10.032

[8] G. Goldring, in *Heavy Ion Collisions*, edited by R. Bock (North-Holland Publishing Company, 1982), Vol. 3, chap. 3, pp. 483–572, ISBN 9780444853523

[9] onsemi, C-Series SiPM Sensors Data Sheet (2022), Rev. 9

[10] Analog Devices, AD8065/AD8066 Data Sheet (2019), Rev. L

[11] C. Mihai, G. Pascovici, G. Ciocan, C. Costache, V. Karayonchev, A. Lungu, N. Mărginean, R.E. Mihai, C. Neacşu, J.M. Régis et al., Development of large area Silicon Photomultipliers arrays for γ-ray spectroscopy applications, Nucl. Instrum. Methods Phys. Res. Sect. A **953**, 163263 (2020). 10.1016/j.nima.2019.163263

[12] Infineon, BAT15-04W Datasheet (2018), v1.0

[13] Analog Devices, AD8012* Data Sheet (2019), Rev. C

[14] B. Wang, H. Wang, D. Wang, X. Zhang, Y. Zhang, L. Zhu, X. Wang, J. Liu, Q. Liu, M. Li et al., Investigation of consistency and temperature compensation in SiPM-coupled GAGG scintillator linear arrays, Nucl. Instrum. Methods Phys. Res. Sect. A **1082**, 171016 (2026). 10.1016/j.nima.2025.171016

[15] M.M. Bé, V. Chisté, C. Dulieu, X. Mougeot, E. Browne, V. Chechev, N. Kuzmenko, F. Kondev, A. Luca, M. Galán et al., Table of Radionuclides, Vol. 5 of *Monographie BIPM-5* (Bureau International des Poids et Mesures, 2010), ISBN 978-92-822-2234-8, http://www.bipm.org/utils/common/pdf/monographieRI/Monographie_BIPM-5_Tables_Vol5.pdf

[16] Y. Luo, L. Ma, D. Xie, Y. Huang, Y. Wang, F. Fang, J. Han, W. Lin, X. Liu, X. Luo et al., Characterization of the energy response of a LYSO+SiPM detector module for $E//B$ NPA using α and hydrogen ions, Nucl. Instrum. Methods Phys. Res. Sect. A **1061**, 169110 (2024). 10.1016/j.nima.2024.169110

[17] B. Singh, A.R. Farhan, Nuclear Data Sheets for $A = 74$, Nucl. Data Sheets **107**, 1923 (2006). 10.1016/j.nds.2006.05.006

[18] S.C. Wu, Nuclear data sheets for $A = 181$, Nucl. Data Sheets **106**, 367 (2005). 10.1016/j.nds.2005.11.001